PSFC/JA-16-10

The Effects of Main-Ion Dilution on Turbulence in Low q_{95} C-Mod Ohmic Plasmas, and Comparisons with Nonlinear GYRO

P. Ennever, M. Porkolab, J. Candy[1], G. Staebler[1], M. L. Reinke[2],
J. E. Rice, J. C. Rost, D. Ernst, J. Hughes, S. G. Baek,
and The Alcator C-Mod Team

[1]General Atomics
[2]ORNL

April, 2016

Plasma Science and Fusion Center
Massachusetts Institute of Technology
Cambridge MA 02139 USA

The Effects of Main-Ion Dilution on Turbulence in Low q_{95} C-Mod Ohmic Plasmas, and Comparisons with Nonlinear GYRO

P. Ennever,[1, a)] M. Porkolab,[1, b)] J. Candy,[2, c)] G. Staebler,[2, d)] M.L Reinke,[3, e)] J. E. Rice,[1, f)] J. C. Rost,[1, g)] D. Ernst,[1, h)] J. Hughes,[1, i)] S. G. Baek,[1, j)] and The Alcator C-Mod Team[1]

[1)] *MIT*

[2)] *General Atomics*

[3)] *ORNL*

Recent experiments on C-mod seeding nitrogen into ohmic plasmas with $q_{95} = 3.4$ found that the seeding greatly reduced long-wavelength (ITG - scale) turbulence. The long-wavelength turbulence that was reduced by the nitrogen seeding was localized to the region of $r/a \approx 0.85$, where the turbulence is well above marginal stability (as evidenced by $Q_i/Q_{\mathrm{GB}} >> 1$). The nonlinear gyrokinetic code GYRO was used to simulate the expected turbulence in these plasmas, and the simulated turbulent density fluctuations and turbulent energy fluxes quantitatively agreed with the experimental measurements both before and after the nitrogen seeding. Unexpectedly, the intrinsic rotation of the plasma was also found to be affected by the nitrogen seeding, in a manner apparently unrelated to a change in the electron-ion collisionality that was proposed by other experiments. This important observation remains the subject of future studies.

Keywords: Tokamak, C-Mod, Gyrokinetics, Validation, GYRO, Dilution, Impurities

a)Electronic mail: ennever@psfc.mit.edu

b)Electronic mail: porkolab@psfc.mit.edu

c)Electronic mail: candy@fusion.gat.com

d)Electronic mail: staebler@fusion.gat.com

e)Electronic mail: mlreinke@psfc.mit.edu

f)Electronic mail: rice@psfc.mit.edu

g)Electronic mail: rost@fusion.gat.com

h)Electronic mail: dernst@psfc.mit.edu

i)Electronic mail: jwhughes@psfc.mit.edu

j)Electronic mail: sgbaek@mit.edu

The Effects of Main-Ion Dilution on Turbulence in Low q_{95} C-Mod Ohmic Plasmas, and Comparisons with N

I. INTRODUCTION

The energy confinement time τ_E in ohmic tokamak plasmas exhibits two characteristic scaling regimes: the low-density linear ohmic confinement (LOC) regime in which the energy confinement time scales linearly with the density, and the high-density saturated ohmic confinement (SOC) regime in which the energy confinement time is independent of the density[1].

Turbulent fluctuations are well-known to be the primary contributor to energy transport in current tokamaks[2]. The magnitude of the energy transport driven by turbulence is influenced by several parameters, in particular the inverse of the local gradient scale-length of the temperature profile normalized to the minor radius: $a/L_T = a\nabla T/T$ where a is the minor radius, and T is the temperature. The relationship between the a/L_T and the turbulence-driven energy flux, Q, is primarily defined by two parameters: a critical gradient (the minimum value of the gradient for the turbulence to become unstable), and a stiffness (the rate of increase of Q with increasing a/L_T when a/L_T is above the critical gradient). The exact values of the stiffness and critical gradient will depend on a number of factors, including the ratio of the main ion species density, in this case deuterium, to the electron density, n_D/n_e.

Main-ion dilution, meaning the reduction of n_D/n_e to less than 1, has been previously found[3,4] in both experiments on the Alcator C-Mod tokamak[5] and simulations with GYRO[6] and TGLF[7] to reduce turbulent energy transport. In particular, dilution in controlled experiments was achieved through seeding of nitrogen gas into ohmic plasmas on C-Mod while a cryopump held the overall electron density fixed throughout the seeding[4]. Those experiments were performed at safety factors q_{95} of 3.9 and 4.5, which corresponded to magnetic fields of 5.4 T, and plasma currents of 0.8 and 1.0 MA, respectively. The nitrogen seeding resulted in a decrease in the turbulent ion energy flux, Q_i with either no change in a/L_{Ti} or an increase in a/L_{Ti} in the experiment, which implies either a change in the stiffness or the critical gradient of the transport. Simulations with GYRO and TGLF predicted that the nitrogen seeding could affect both the stiffness and the critical gradient of the turbulence, and the simulated energy fluxes quantitatively agreed with the experimental measurements in cases where the turbulence was above marginal stability[4]. In this paper, we extend these experiments to higher plasma currents and lower values of q_{95}, which resulted in higher

electron densities and temperatures in both the LOC and SOC regimes. It also resulted in larger Doppler shifts of turbulence measured in the lab frame, which made possible quantitative comparisons between measured density fluctuations and density fluctuations with GYRO simulations. This provides a valuable addition to the previous dilution study[4], which compared the measured and GYRO-simulated ion and electron energy transport.

The remainder of the paper is organized as follows: Section II describes nitrogen seeding experiments performed on low-q_{95} ohmic plasmas on Alcator C-Mod, while Section III describes the measurements of density fluctuations in the experiments described in Section II. Section IV describes comparisons between measured and simulated energy fluxes and density fluctuations from the experiments in Section II. Section V describes the investigation of the effect of nitrogen seeding on the intrinsic rotation from the experiments in Section II. Finally, Section VI summarizes the work and discusses the broader implications of the results.

II.   LOW q_{95} NITROGEN SEEDING EXPERIMENTS ON C-MOD

The experiments described in this section were all performed in ohmic plasmas on Alcator C-Mod with a toroidal field of 5.4 T, with electron densities that were held fixed during a shot and scanned shot-to-shot. Electron densities were scanned through both the LOC and SOC regimes, from the minimum density in which there were not significant runaway electrons, up to the maximum density in which the addition of nitrogen did not cause poloidal detachment[8] (which caused loss of density control and often a disruption). Time traces of important experimental parameters for three representative plasmas are shown in Fig. 1. The traces show that the density and magnetic geometry are held constant throughout the seeding (Figs. 1a and 1b), but the seeding increases the radiated power and nitrogen brightness (Figs. 1d and 1e) and also effects the ion temperature and ion intrinsic rotation (Figs. 1c and 1f).

The electron density and the amount of nitrogen seeding were held constant within a shot, and scanned shot-to-shot. The electron density values of the scan cover both the LOC and SOC regimes and are shown in Fig. 2 which display the density and energy confinement time values from the scan both before and after the nitrogen seeding. The energy confinement time was calculated by dividing the stored energy by the difference between the ohmic input power and the time-derivative of the stored energy. The seeding did not seem to result in

a systematic increase in the energy confinement time, but that does not imply that there was no change in the turbulent energy transport. Rather, it implies that the increase in the radiated power lost from the seeding (shown in Fig. 1d) was offset by a decrease in the turbulent transport. This is similar to what was observed in the previous nitrogen seeding experiments on C-Mod[4].

III. DENSITY FLUCTUATION MEASUREMENTS OF SEEDED AND UNSEEDED PLASMAS

Alcator C-Mod has several diagnostics that monitor fluctuations, but the phase contrast imaging diagnostic, PCI, is an absolutely calibrated instrument that measures the line-integral of density fluctuations along the path of a laser beam[9]. The PCI system on Alcator C-Mod images density fluctuations along 32 vertical chords onto a liquid nitrogen cooled HgCdTe photoconductive detector, as shown in Fig. 3. These chords pass through the top and the bottom of the plasma column, and fluctuations from the core and edge regions are added together along each chord. Although this makes the interpretation of the signal non-trivial, and requires a synthetic diagnostic to compare to GYRO simulations, the other advantages of the PCI diagnostic (very high signal-to-noise ratio, an absolutely calibrated signal, and determination of the wavenumber spectrum) make it very valuable for measuring turbulence. The PCI system was upgraded before the 2015 Alcator C-Mod campaign with a new detector that has a better frequency response than that used in earlier publications[3]. The new detector is much more sensitive to higher frequency fluctuations, having the same response at frequencies that are about twice as high as the earlier detector. Results presented in this paper were obtained with this new system.

The PCI signal was monitored in both the seeded and unseeded phase of the discharges, and it was observed that the seeding significantly reduced the high-frequency portion of the PCI spectrum as shown in Fig. 4. There was a particular wing-like feature that was clearly visible at low-wavenumbers ($|k_R| \leq 10$ cm^{-1}) and high-frequencies ($f \geq 100$ kHz). This reduction due to the seeding was robustly observed in both the LOC and SOC regimes, and was observed even when there were not substantial changes to the rotation profile. This is shown in Fig. 5, wherein the change in the amplitude of this high-frequency feature is shown to be larger in every case with the nitrogen seeding.

The narrow phase-velocity of the feature implies that the feature originates from a relatively narrow radial region of the plasma. The origin of this feature cannot be determined solely through the PCI signal, however there is another density fluctuation diagnostic, the O-mode reflectometer[10], which measures density fluctuations on the outboard midplane at a region with a particular electron density where the launched wave frequency matches the electron plasma frequency: $f_{\text{reflect}} = f_{pe} = 8.98 \times \sqrt{n_{20}}$ where n_{20} is the electron density in units of 10^{20}m^{-3}. For a monotonically increasing density profile (as was seen in the experiments) these particular electron densities correspond to particular radial locations in the plasma. The reflectometer has channels measuring fluctuations at frequencies of 50, 60, 75, 88, 110, 121, and 140 GHz, which correspond to densities of $n_{20} = 0.31$, 0.45, 0.70, 0.96, 1.5, 1.82, and 2.4, respectively. Despite the fact that the PCI and the reflectometer are measuring fluctuations at both poloidally and toroidally separated locations, it is still useful to compare the two measurements. This is due to the fact that the turbulence of interest is going to be toroidally symmetric, and while the turbulent fluctuations will be poloidally asymmetric, the eigenmodes will typically extend from the outer midplane to the top and bottom of the plasma column[2].

When the fluctuations measured by the PCI and the reflectometer were compared in the seeded and unseeded phases of the experiment, the reflectometer channel measuring fluctuations at r/a = 0.85 displays a similar decrease in high-frequency fluctuations as the PCI spectrum and over a similar timescale. This is shown in Fig. 6. It also shows that the timescale of the decrease in fluctuations is somewhat faster than the overall saturation of the nitrogen brightness in the plasma, which is also consistent with these fluctuations originating from closer to the edge of the plasma. The reflectometer channel measuring fluctuations at r/a = 0.6 also shows a decrease in the high frequency part of the spectrum, but there is less of a change, and it changes over a longer timescale as compared to the PCI spectrum. This radial location, $0.8 \leq r/a \leq 0.9$, was robustly observed to be the only location where the reflectometer measured fluctuations show a similar magnitude decrease to fluctuations measured by PCI. This is shown in Fig. 7, which plots the ratio of the power in the high-frequency fluctuations in the unseeded phase to the power in the high-frequency fluctuations in the seeded phase for three different densities. A value of 1 indicates that there was no change in the high-frequency fluctuations with the seeding, while a value greater than one indicates that the seeding caused a decrease in the high-frequency fluctuations. In all

three density cases, the reflectometer channels looking at $0.8 \leq r/a \leq 0.9$ showed a decrease in fluctuations with seeding that was comparable to the decrease observed with the PCI diagnostic. This radial location is where the turbulence is well above marginal stability, as discussed in Ref. 4, thus this result is consistent with the nitrogen seeding having a stabilizing effect on the turbulence through dilution.

IV. GYROKINETIC SIMULATIONS OF SEEDED AND UNSEEDED PLASMAS, AND COMPARISONS WITH EXPERIMENTAL MEASUREMENTS

Once the PCI measurements were localized to a particular minor radial location, they could be compared to the output of a local nonlinear GYRO simulation[6]. The PCI diagnostic is absolutely calibrated and measures both the frequency and wavenumber spectra of the turbulence, which makes it an excellent tool for the validation of gyrokinetic codes. Local nonlinear GYRO outputs, among other things, the turbulent density fluctuation amplitudes and energy fluxes near a particular value of the minor radius. This can be compared to the PCI measurements through the use of a synthetic PCI diagnostic[11] which performs the line-integration of the GYRO density fluctuations and includes the experimental geometry and system response. This enables a quantitative comparison of the experimental PCI frequency-wavenumber spectra to the simulation. Thanks to the analysis comparing the reflectometer and PCI fluctuation measurements in the previous section, there is a particular turbulent feature that can be compared to GYRO simulations.

In order to compare the PCI spectra measured in the experiment to the synthetic PCI spectra computed from a local nonlinear GYRO simulation, the portion of the experimental spectrum originating from a specific location in the plasma must be isolated. To do this, the high-frequency, low-wavenumber feature was isolated from the rest of the PCI spectrum, as shown in Fig. 8. This was done by selecting a fixed phase velocity (shown in the solid white lines) and a specific wavenumber window (shown in the dashed white lines), and subtracting the value of the spectrum at the edge of the window from the spectrum inside the window. This analysis is also restricted to frequencies above 150 kHz, because that is where the feature is most prominent above the rest of the spectrum. This method assumes that the feature is coming from a different radial region from the remainder of the PCI spectrum,

TABLE I. Table of total energy fluxes at r/a = 0.85 for the unseeded and seeded phases of an LOC discharge from the $q_{95} = 3.4$ experiment used for the comparison between the GYRO simulated and experimentally measured density fluctuations. The experimental energy flux is computed by TRANSP from power balance. All energy fluxes are in Gyrobohm units, where $Q_{\mathrm{GB}} = n_e T_e c_s (\rho_s/a)^2$, where n_e is the electron density, T_e is the electron temperature, $c_s = \sqrt{T_e/m_i}$ is the sound speed, $\rho_s = c_s/(eB/(m_D c))$ is the ion sound gyroradius, and a is the minor radius.

Phase of Discharge	Exp. Energy Flux (GB Units)	GYRO Energy Flux (GB Units)
Unseeded	60 ± 12	52
Seeded	45 ± 15	45

which is supported by the reflectometer measurements in Sec. III.

Local nonlinear GYRO simulations were performed for r/a = 0.85 for a simulation in the seeded and unseeded phase of the plasma discharge. The measured electron and ion temperature profiles, as well as the measured electron temperature profile, were used in the simulation. For the seeded phase, the electron temperature profile inverse gradient scale length, a/L_{Te}, input to the GYRO simulation was reduced by 20% compared to the experimental measurements in order to bring the experimental and simulated energy fluxes into agreement. This change in a/L_{Te} is within the experimental uncertainties. Table I shows the values of the simulated and experimental energy fluxes in gyrobohm units, and shows that they are in agreement within the uncertainties. The experimental energy fluxes were computed by TRANSP[12]. Figure 9 shows the comparison between the spectra after the background subtraction (same as in Fig. 8) and the synthetic PCI spectra from the local GYRO simulations.

The comparison between the experimental PCI spectra and the synthetic PCI spectra from GYRO in both the seeded and unseeded phase is depicted in Fig. 10, which shows that the experiment and simulation are quantitatively consistent in both phases. This is a particular LOC case from the experiments which had the best ion temperature profile measurements. The comparison in Fig. 10 is on an absolute scale, and demonstrates that GYRO can predict both the density fluctuations and energy fluxes due to turbulence. The main uncertainties of the synthetic PCI calculation are the radial width of the turbulence (which was found to be approximately $0.8 \leq r/a \leq 0.9$ using the reflectometer) and the

$\vec{E} \times \vec{B}$ velocity (which was measured, but with significant uncertainty at that radial location). The uncertainty in the radial width is reflected in the error bars in Fig. 10. The uncertainty in the $\vec{E} \times \vec{B}$ velocity was accounted for by performing multiple synthetic PCI analyses with different $\vec{E} \times \vec{B}$ velocity values, and the one most consistent with the experiment was chosen. The value of the $\vec{E} \times \vec{B}$ velocity was different in the unseeded and seeded phases, but both are consistent with the experimental measurements. The uncertainty in the experimental PCI signal is almost entirely due to the uncertainty in the absolute calibration, which is a fixed value that is the same for both the seeded and unseeded portions and affects only the magnitude but not the shape of the spectra.

V. EFFECTS OF NITROGEN SEEDING ON INTRINSIC ROTATION

In addition to investigating the effect of dilution on turbulent energy flux, the nitrogen seeding experiments also allowed for the study of the dependencies of the intrinsic rotation. Earlier studies of intrinsic rotation in ohmic plasmas found that the direction of rotation depended on a critical value of the product of the electron density and the edge safety factor, $n_e q_{95}$, that was close to the LOC-SOC transition critical $n_e q_{95}$[13]. Previous seeding experiments at lower plasma currents and higher q_{95} values found that the nitrogen seeding affected the intrinsic rotation[4]. In particular, the nitrogen seeding caused plasmas with a $n_e q_{95}$ value above the critical value to reverse the direction of their intrinsic rotation from counter-current to co-current. This phenomena was also observed in the high-current, low-q_{95} plasmas discussed in Sec. II. With the data from both sets of experiments, a more systematic study of the intrinsic rotation could be carried out.

Studies on several tokamaks, including both Alcator C-Mod and ASDEX-U, found that the intrinsic rotation direction in tokamaks correlates with the effective collisionality, $\nu_{\mathrm{eff}} \approx R \, Z_{\mathrm{eff}} n_e / (T_e)^2$ the ratio of the electron-ion collision frequency to the curvature drift frequency, where R is the major radius in m, n_e is the plasma density in units of $10^{20} \mathrm{m}^{-3}$, and T_e is the electron temperature in keV[14,15,16]. Figure 11 shows the intrinsic rotation direction and the ν_{eff} for both unseeded and nitrogen seeded plasmas. It clearly shows that the seeded and unseeded plasmas have different critical values of ν_{eff}, which implies that ν_{eff} is not capturing the physics of the seeding-induced change in the intrinsic rotation, at least not fully. A parameter that does seem to separate the co-current rotating and counter-current

rotating plasmas in both the seeded and unseeded cases is the product of the deuterium density and the edge safety factor, $n_D q_{95}$. This is shown in Fig. 12, which displays the core rotation and $n_D q_{95}$ values of unseeded and seeded plasmas for three different values of q_{95}. It shows that there is a value of $n_D q_{95} \approx 4$ which separates the co-current and counter-current rotating plasmas. The horizontal error bars in Fig. 12 represent the uncertainties in the impurity species density, which effects the value of n_D which was calculated based on the impurity species densities and electron density. This suggests that the ion dynamics are more responsible for the seeding-induced rotation change than the electron dynamics, since it is the ion density rather than the electron density that determines the rotation direction. Because of the significant error bars and scatter in the data, more experimental results would be desirable for a definitive answer.

VI. SUMMARY AND CONCLUSIONS

In this paper we explored the impact of nitrogen seeding on turbulence through controlled experiments in the Alcator C-Mod tokamak and simulations using the GYRO code at a higher value of the plasma current and a lower value of q_{95} than in previous experiments[4], which enabled quantitative comparisons between measured and GYRO-simulated density fluctuations. In these experiments, the density fluctuations showed a significant decrease due to the nitrogen seeding, and the GYRO simulations quantitatively agree with both the measured energy fluxes and density fluctuations in both the seeded and unseeded phases of the plasma discharge. This provides a useful validation of the GYRO code and its treatment of the effect of impurity species on turbulence in regions where the long-wavelength turbulence ($k_\theta \rho_s < 1$) is well above marginal stability, in this case in the vicinity of r/a = 0.85.

The fact that the fluxes and fluctuations both quantitatively agree simultaneously between the GYRO simulations and the experimental measurements gives greater confidence that the simulations are properly capturing the physics of the turbulence in these cases. It therefore also gives great confidence in the result from Ref.[4] namely that main-ion dilution (meaning the reduction of n_D/n_e to less than 1) has a significant stabilizing effect on ITG turbulence which results in reduced energy transport. It was also found that main ion dilution reduced the ion energy transport stiffness and increased the critical ion temperature

gradient in the GYRO simulations. Main ion dilution is expected to be present in future fusion reactor plasmas such as in ITER, so this effect would result in a reduction in energy transport and an increase in equilibrium ion temperature. Nitrogen seeding may not be suitable for a burning plasma environment, however, so further work on other medium-Z impurity species like neon would be beneficial to establish confidence in extrapolation to future fusion devices such as ITER.

The effects of the seeding on intrinsic rotation are also relevant to future fusion devices, as they will have very little external momentum input. The physical mechanisms behind intrinsic rotation in tokamak plasmas is still an open area of research, but these experiments provide a very valuable data set to future investigations. The result that the change in the intrinsic rotation was not strictly related to a change in the electron collisionality (only) shows that there must be another dependency. The parameter that was found to unify the data best was $n_D q_{95}$, which is related to the ion-ion collisionality. This could be related to the model proposed by Barnes et. al.[17] and studied on MAST[18] which does point to the ion-ion collisionality as an important parameter in the intrinsic momentum transport (and therefore intrinsic rotation). More extensive experimental data and a more detailed theoretical comparison would be necessary to see which model correctly predicts the experimental rotation, but that is left for future work.

VII.   ACKNOWLEDGMENTS

VIII.   FIGURES

REFERENCES

[1]M. Greenwald, D. Gwinn, S. Milora, J. Parker, R. Parker, S. Wolfe, M. Besen, F. Camacho, S. Fairfax, C. Fiore, M. Foord, R. Gandy, C. Gomez, R. Granetz, B. Labombard,
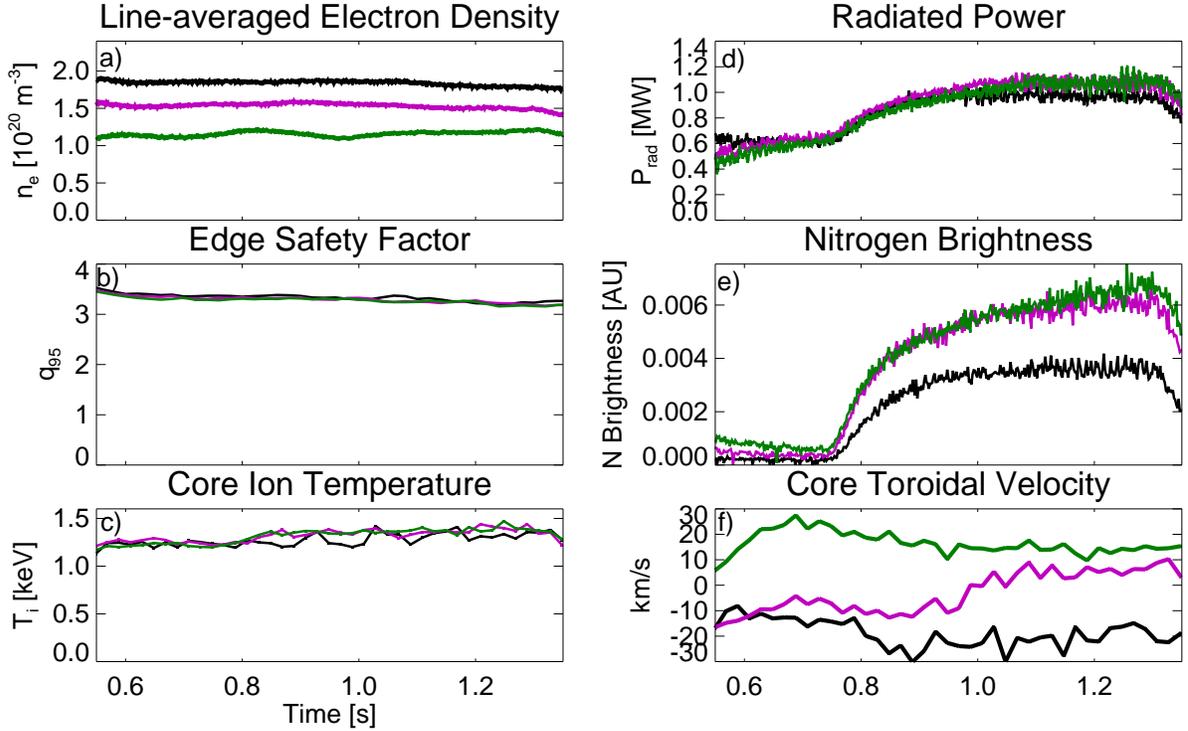
FIG. 1. Plots of the experimental time traces for three representative discharges in the low-q_{95} experiments. The three colors correspond to different n_e values, as shown in plot a). Plot b) shows the q_{95} values for the three discharges. Plot c) shows the core ion temperature which was measured using an X-ray crystal spectrometer looking at Argon. Plot d) shows the total radiated power. Plot e) shows the line brightness of nitrogen. Plot f) shows the core toroidal ion velocity which was measured using an X-ray crystal spectrometer looking at Argon. Positive toroidal velocity corresponds to co-current rotation, and negative toroidal velocity corresponds to counter-current rotation.

B. Lipschultz, B. Lloyd, E. Marmar, S. Mccool, D. Pappas, R. Petrasso, P. Pribyl, J. Rice, D. Schuresko, Y. Takase, J. Terry, and R. Watterson, Physical review ... **53**, 352 (1984).

[2]W. Horton, Reviews of Modern Physics **71**, 735 (1999).

[3]M. Porkolab, J. Dorris, P. Ennever, C. Fiore, M. Greenwald, A. Hubbard, Y. Ma, E. Marmar, Y. Podpaly, M. L. Reinke, J. E. Rice, J. C. Rost, N. Tsujii, D. Ernst, J. Candy, G. M. Staebler, and R. E. Waltz, Plasma Phys. Control. Fusion **54**, 124029 (2012).

[4]P. Ennever, M. Porkolab, J. Candy, G. Staebler, M. L. Reinke, J. E. Rice, J. C. Rost, D. Ernst, C. Fiore, J. Hughes, J. Terry, and A. C.-M. Team, Physics of Plasmas **22**, (2015).
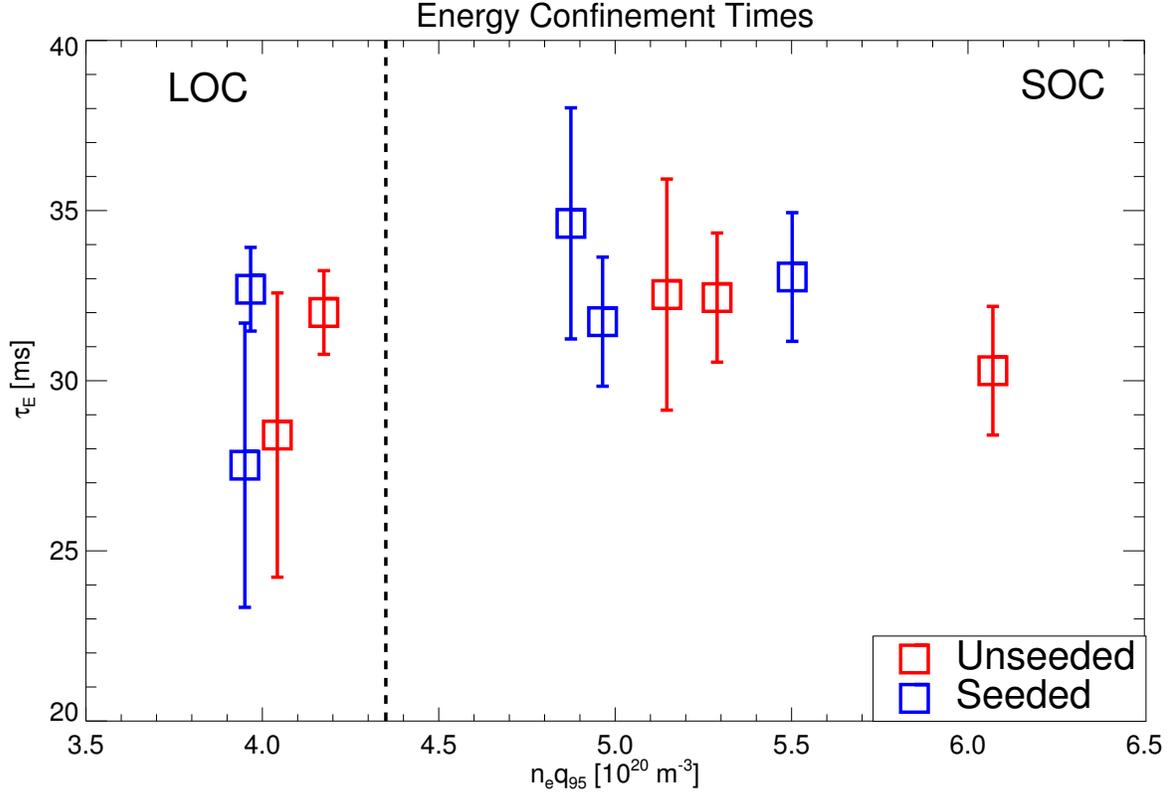
FIG. 2. Plot of the energy confinement times, τ_E for the discharges in the low-q_{95} experiments in both the unseeded phase (in red) and the seeded phase (in blue).

[5]M. Greenwald, D. Andelin, N. Basse, S. Bernabei, P. Bonoli, B. Böse, C. Boswell, R. Bravenec, B. Carreras, I. Cziegler, E. Edlund, D. Ernst, C. Fasoli, M. Ferrara, C. Fiore, R. Granetz, O. Grulke, T. Hender, J. Hosea, D. H. Howell, A. Hubbard, J. Hughes, I. Hutchinson, A. Ince-Cushman, J. Irby, B. LaBombard, R. LaHaye, L. Lin, Y. Lin, B. Lipschultz, J. Liptac, S. Lisgo, A. Lynn, E. Marmar, K. Marr, D. R. Mikkelsen, R. Mc-Dermott, D. Mossessian, A. Parisot, R. Parker, C. Phillips, P. Phillips, M. Porkolab, M. Redi, J. Rice, W. Rowan, M. Sampsell, G. Schilling, S. Scott, J. T. Scoville, N. Smick, J. Snipes, P. Stangeby, V. Tang, J. Terry, M. Ulrickson, G. Wallace, D. Whyte, J. Wilson, J. Wright, S. Wolfe, S. Wukitch, B. Youngblood, H. Yuh, K. Zhurovich, and S. Zweben, Nucl. Fusion **45**, S109 (2005).

[6]J. Candy and R. Waltz, Physical Review Letters **91**, 045001 (2003).

[7]G. M. Staebler, J. E. Kinsey, and R. E. Waltz, Physics of Plasmas **14**, 055909 (2007).

Shot= 1120615015 Time= 0.960 Ip = 1.03
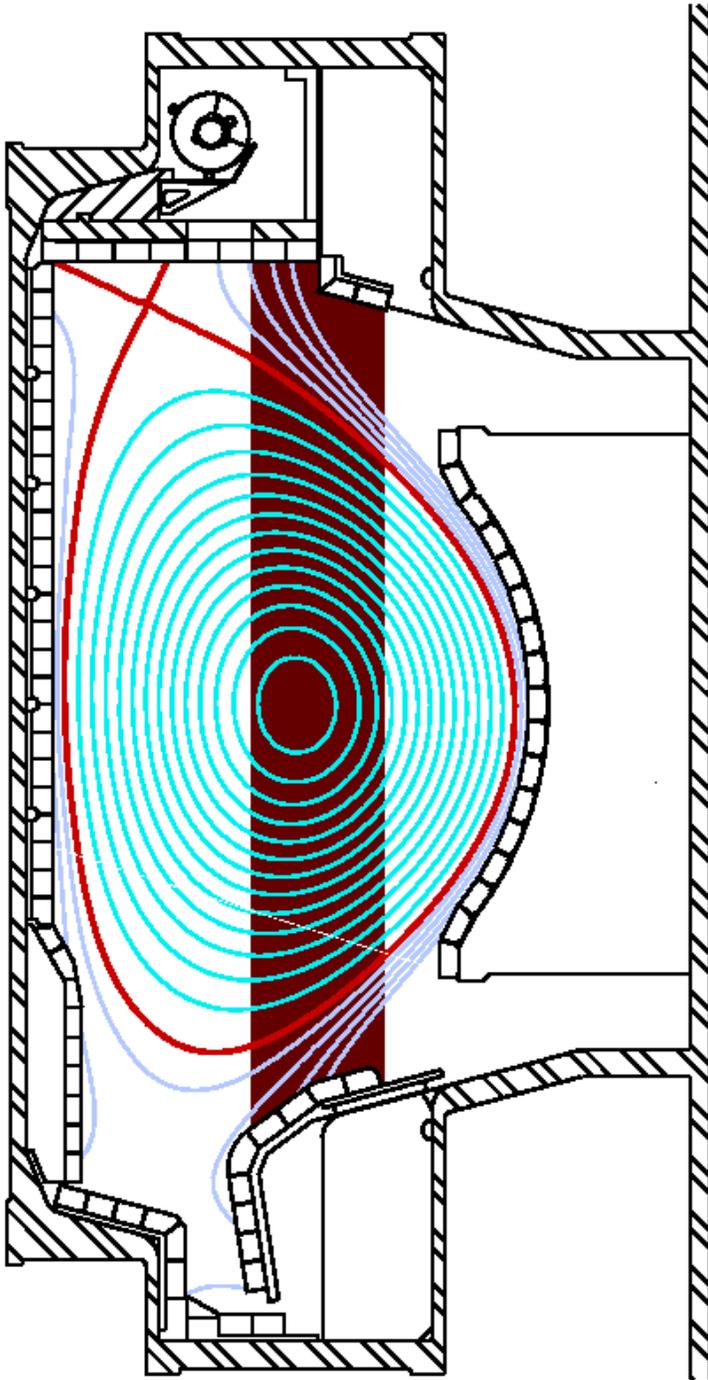
FIG. 3. Diagram of PCI laser beam path through the plasma overlayed on a crossection of the tokamak. This particular magnetic geometry is the same as used for all the plasmas described in this paper.
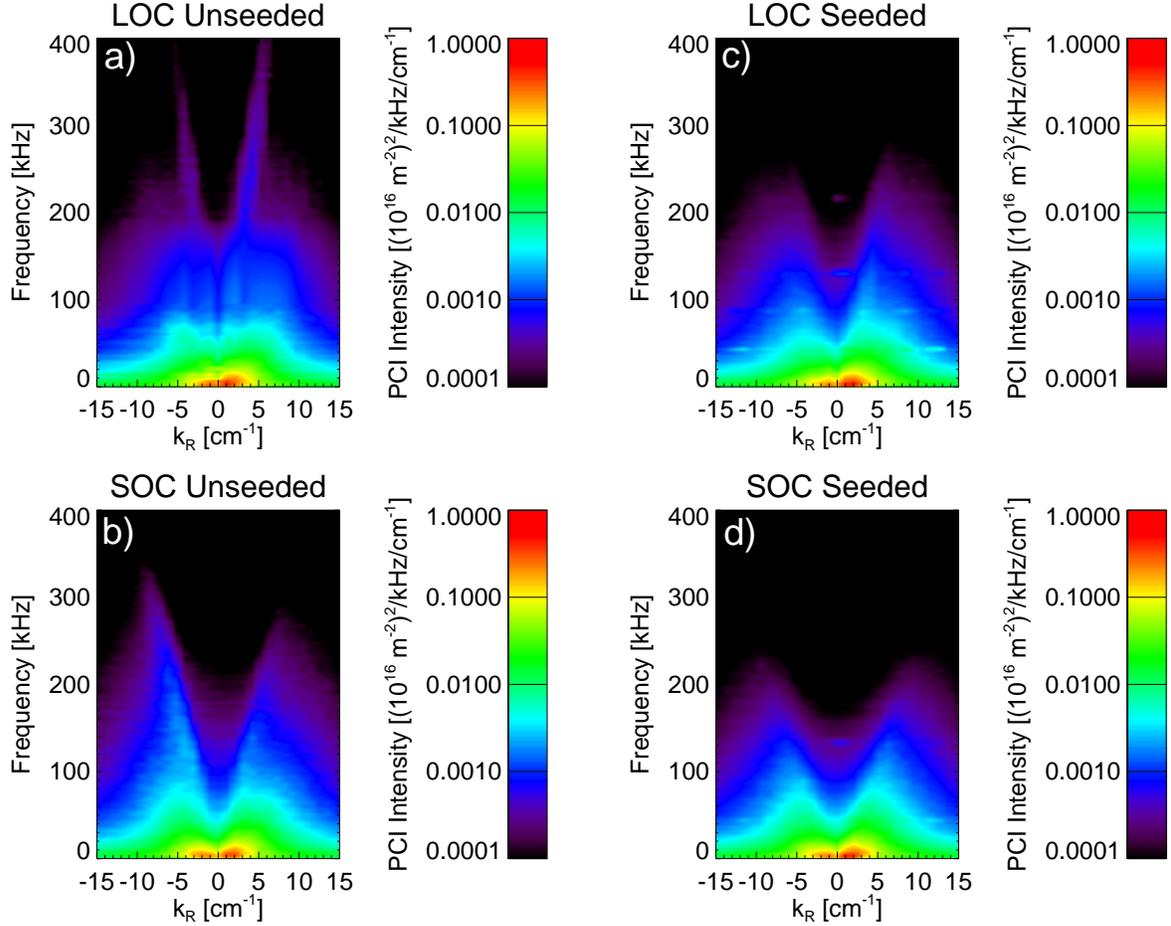
FIG. 4. Plots of PCI measured density fluctuation frequency-wavenumber spectra for a plasma with a density in the LOC regime (top) and a plasma with a density in the SOC regime (bottom), before the seeding (left) and after the seeding (right).

[8]J. A. Goetz, C. Kurz, B. LaBombard, B. Lipschultz, A. Niemczewski, G. M. McCracken, J. L. Terry, R. L. Boivin, F. Bombarda, P. Bonoli, C. Fiore, S. Golovato, R. Granetz, M. Greenwald, S. Horne, A. Hubbard, I. Hutchinson, J. Irby, E. Marmar, M. Porkolab, J. Rice, J. Snipes, Y. Takase, R. Watterson, B. Welch, S. Wolfe, C. Christensen, D. Garnier, D. Jablonski, D. Lo, D. Lumma, M. May, A. Mazurenko, R. Nachtrieb, P. OShea, J. Reardon, J. Rost, J. Schachter, J. Sorci, P. Stek, M. Umansky, and Y. Wang, Physics of Plasmas **3**, 1908 (1996).

[9]M. Porkolab, J. C. Rost, N. Basse, J. Dorris, E. Edlund, L. Lin, Y. Lin, and S. Wukitch, Plasma Science, IEEE Transactions on **34**, 229 (2006).
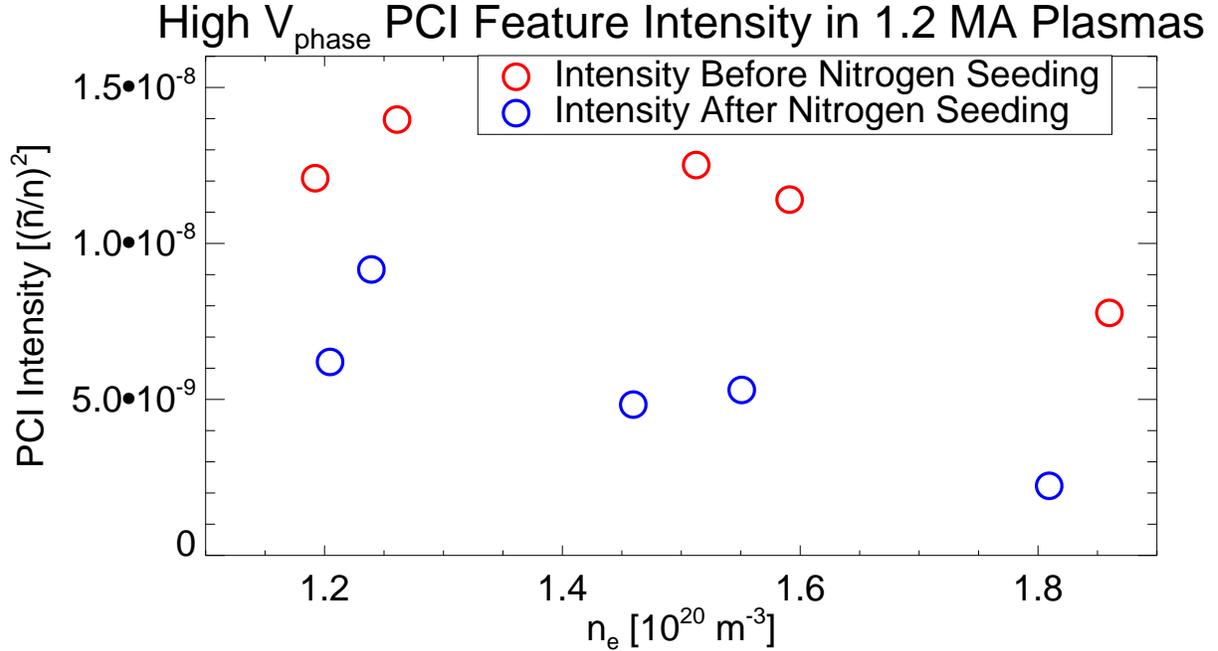
FIG. 5. Plot of the amplitude of the high phase-velocity feature of the PCI spectra before nitrogen seeding (red) and after nitrogen seeding (blue). The magnitude of the feature was computed by integrating the frequency-wavenumber spectrum along a fixed phase velocity ($f/|k| = $ const) with $f > 100$ 100 kHz.

[10]N. P. Basse, A. Dominguez, E. M. Edlund, C. L. Fiore, R. S. Granetz, A. E. Hubbard, J. W. Hughes, I. H. Hutchinson, J. H. Irby, B. LaBombard, L. Lin, Y. Lin, B. Lipschultz, J. E. Liptac, E. S. Marmar, D. A. Mossessian, R. R. Parker, M. Porkolab, J. E. Rice, J. A. Snipes, V. Tang, J. L. Terry, S. M. Wolfe, S. J. Wukitch, K. Zhurovich, R. V. Bravenec, P. E. Phillips, W. L. Rowan, G. I. Kramer, G. Schilling, S. D. Scott, and S. J. Zweben, Fusion Science and Technology **51**, 476 (2007).

[11]J. C. Rost, L. Lin, and M. Porkolab, Physics of Plasmas **17**, 062506 (2010).

[12]R. Goldston, D. McCune, H. Towner, S. Davis, R. Hawryluk, and G. Schmidt, Journal of Computational Physics **43**, 61 (1981).

[13]J. E. Rice, I. Cziegler, P. H. Diamond, B. P. Duval, Y. a. Podpaly, M. L. Reinke, P. C. Ennever, M. J. Greenwald, J. W. Hughes, Y. Ma, E. S. Marmar, M. Porkolab, N. Tsujii, and S. M. Wolfe, Physical Review Letters **107**, 265001 (2011).

[14]J. E. Rice, M. J. Greenwald, Y. a. Podpaly, M. L. Reinke, P. H. Diamond, J. W. Hughes, N. T. Howard, Y. Ma, I. Cziegler, B. P. Duval, P. C. Ennever, D. Ernst, C. L. Fiore,
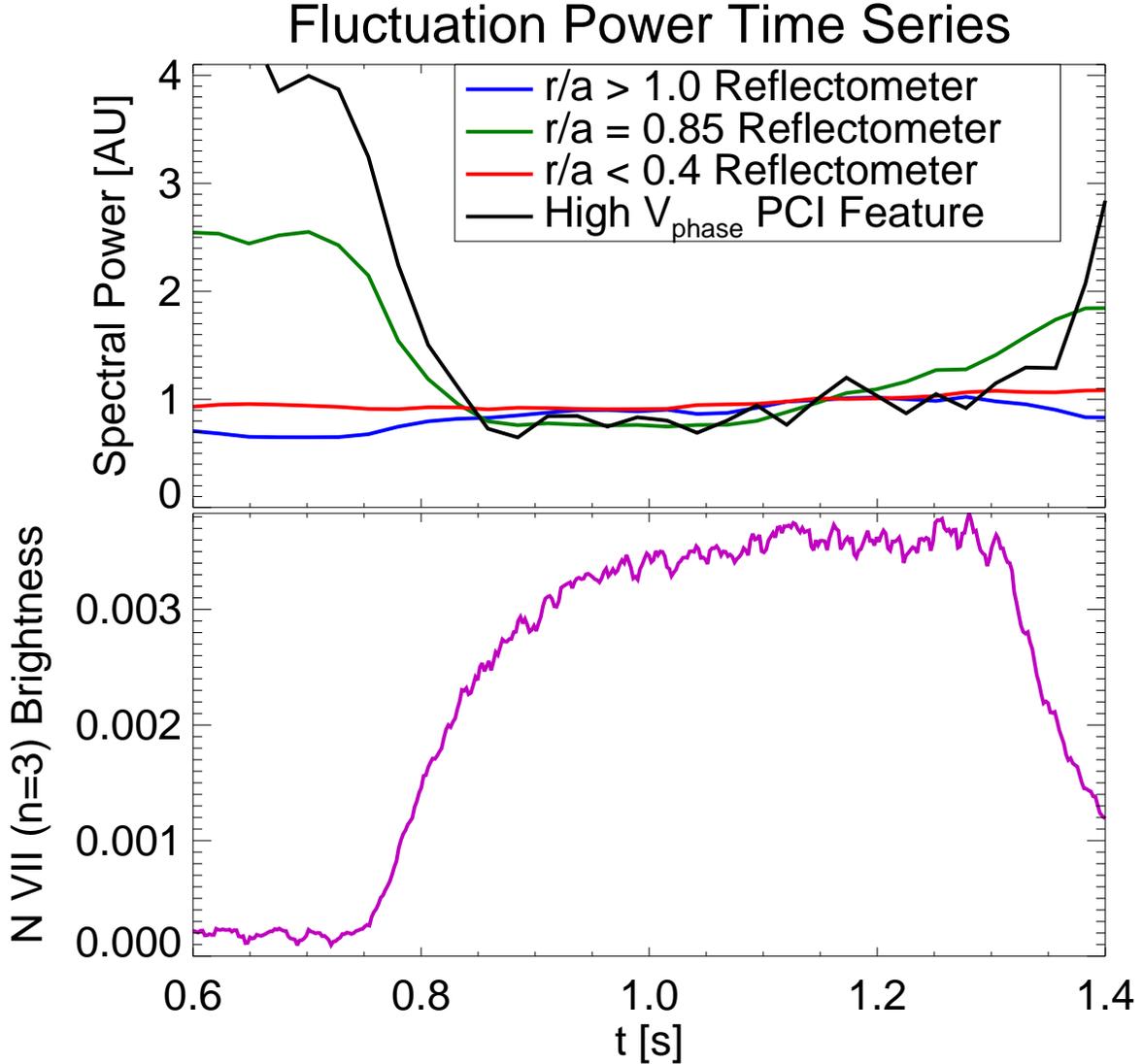
FIG. 6. Plot of the total power of the F ¿ 150 kHz fluctuations observed by PCI (black), and reflectometer channels looking at r/a ¿ 1.0 (blue), r/a = 0.85 (green), r/a = 0.65 (gold), and r/a ¡ 0.4 (red) on top. The spectral powers have been rescaled such that the fluctuation intensity for t ∈ [1.1s, 1.2s] is equal to 1, for ease of comparison. The bottom plot shows the nitrogen line brightness for reference, to show when the seeding happens.

C. Gao, J. H. Irby, E. S. Marmar, M. Porkolab, N. Tsujii, and S. M. Wolfe, Physics of Plasmas **19**, 056106 (2012).

[15]M. L. Reinke, J. E. Rice, A. E. White, M. Greenwald, N. T. Howard, P. Ennever, C. Gao, A. E. Hubbard, and J. W. Hughes, Plasma Physics and Controlled Fusion **55**, 012001
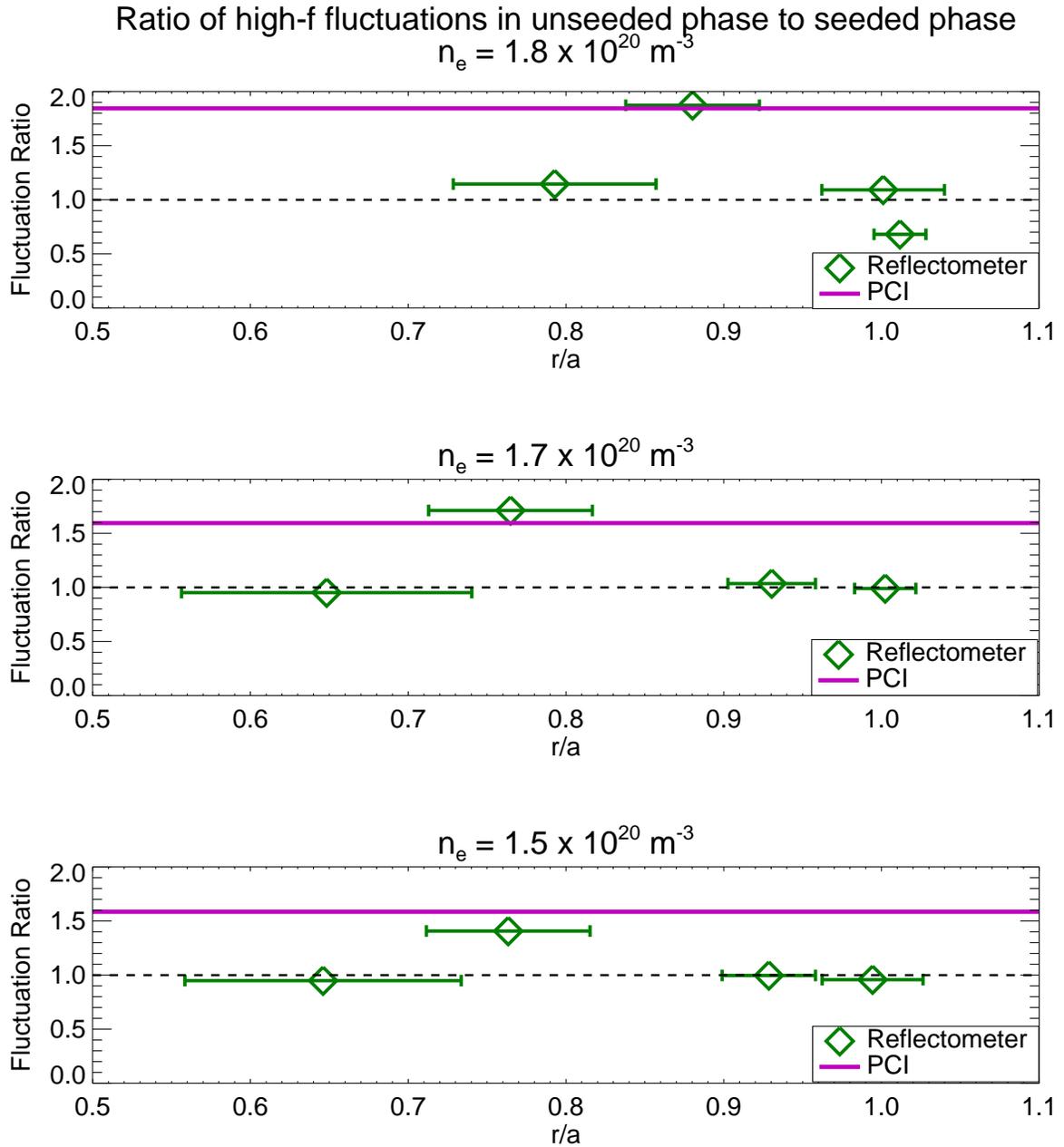
FIG. 7. Plots of the ratio between the high-frequency (f ¿ 150 kHz) portions of the density fluctuation spectra in the unseeded portion of the discharge and the seeded portion of the discharge. The fluctuation ratio from the reflectometer channels are shown in the green diamonds. The fluctuation ratio from PCI is indicated by the purple line (because PCI is not radially localized, therefore there is no radial information). The black dashed line indicates the case of no change in high-frequency fluctuations with the nitrogen seeding. The three plots indicate three different densities, with the top two plots corresponding to plasmas with densities being in the SOC regime and the bottom plot corresponding to a plasma with a density in the LOC regime.
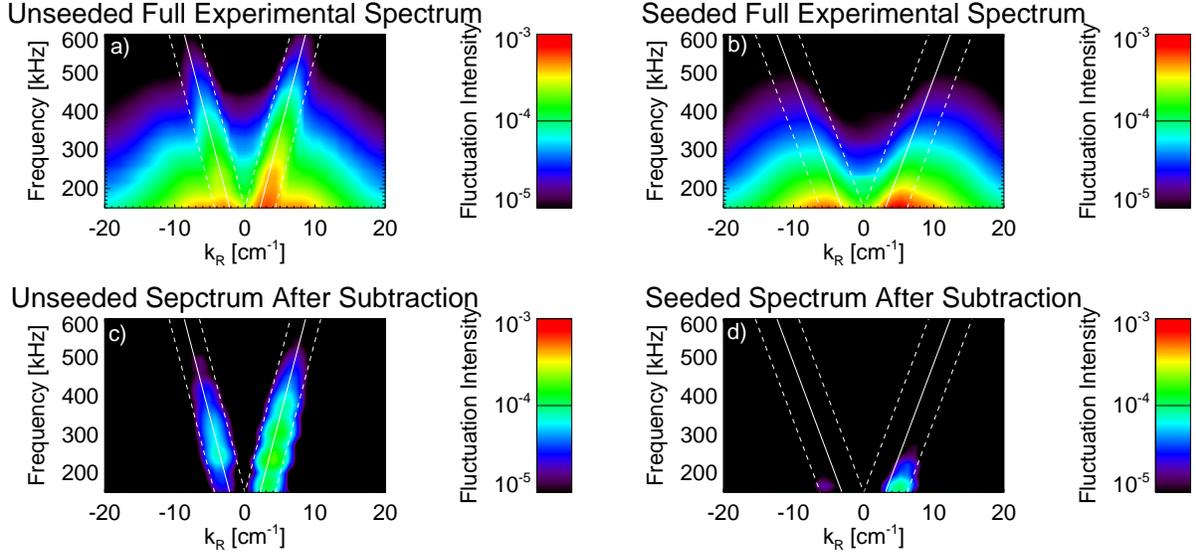
FIG. 8. Plots of the experimental PCI spectra in the unseeded (a) and seeded (b) phases, and of the experimental spectra with the background subtracted isolating the high phase-velocity feature in the unseeded (c) and seeded (d) phases. The white lines indicate center of the feature window (solid line) and the boundaries of the feature window (dashed lines). All plots are on the same scales. These spectra were measured in a LOC plasma.

(2013).

[16] R. McDermott, C. Angioni, R. Dux, E. Fable, T. Pütterich, F. Ryter, A. Salmi, T. Tala, G. Tardini, and E. Viezzer, Plasma Physics and Controlled Fusion **53**, 124013 (2011).

[17] M. Barnes, F. I. Parra, J. P. Lee, E. a. Belli, M. F. F. Nave, and a. E. White, Physical Review Letters **111**, 055005 (2013).

[18] J. Hillesheim, F. Parra, M. Barnes, N. Crocker, H. Meyer, W. Peebles, R. Scannell, and a. Thornton, Nuclear Fusion **55**, 032003 (2015), arXiv:1407.2121v2.
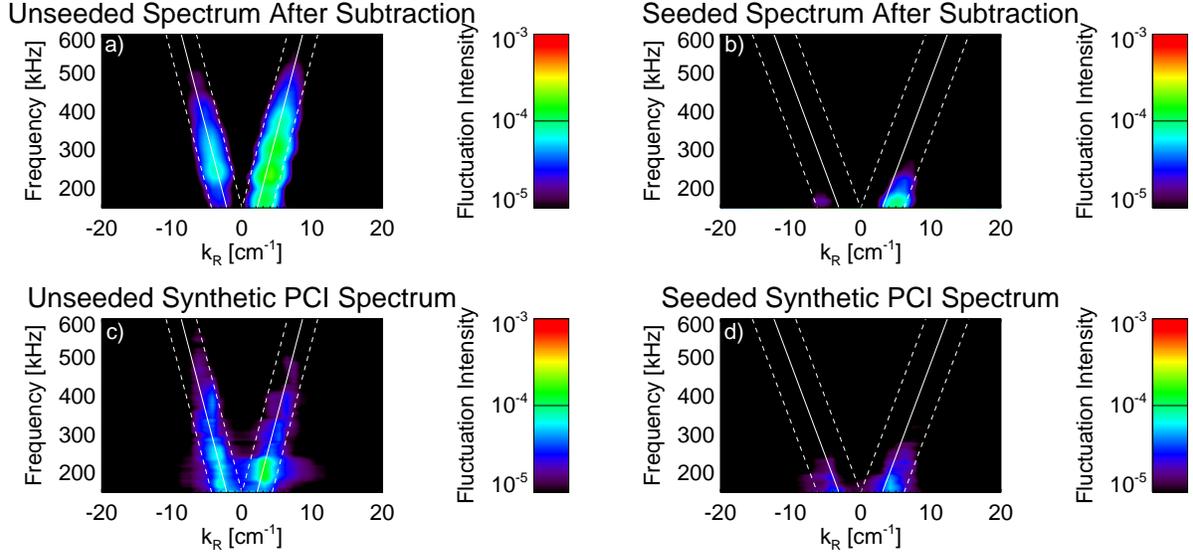
FIG. 9. Plots of the PCI spectrum after subtraction in the unseeded (a) and seeded phase (b), which are the same as Fig 8 (c) and (d). Below are plots of the synthetic PCI spectrum for local GYRO simulations in the unseeded (c) and seeded (d) phase. All plots are on the same scales. The white lines indicate the averaging window used for the quantitative comparison in Fig. 10. All plots are on the same scales. These spectra were measured in a LOC plasma, and the simulation is of the same LOC plasma.
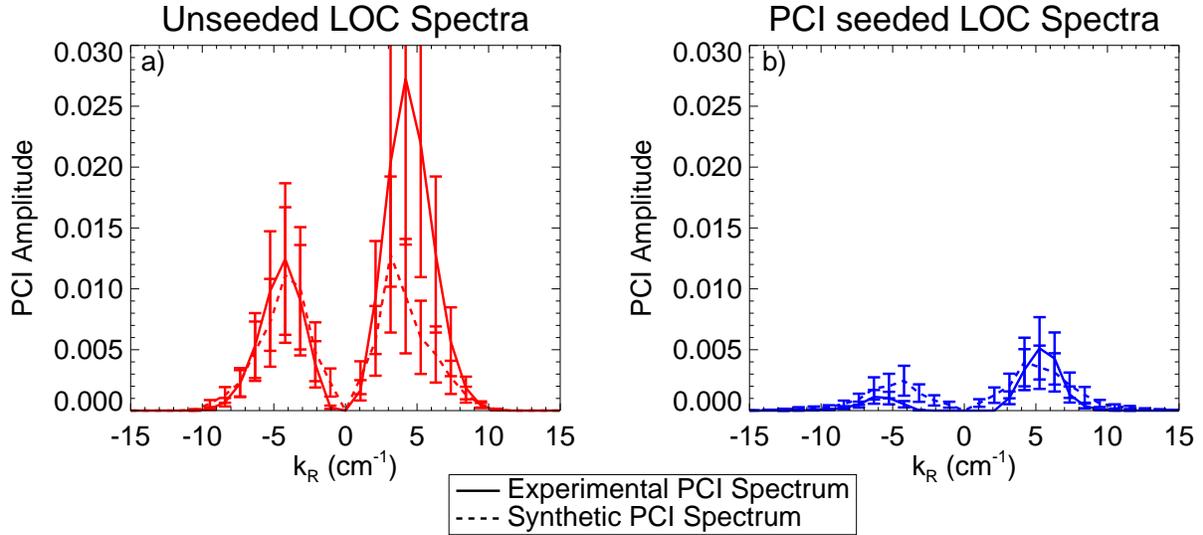
FIG. 10. Plots of the experimental (solid lines) and synthetic (dashed lines) PCI wavenumber spectra in the unseeded phase (a) and seeded phase (b). The wavenumber spectra are computed by averaging between the dashed lines in Fig. 9 for frequencies between 150 kHz and 600 kHz. Both plots are on the same scales.
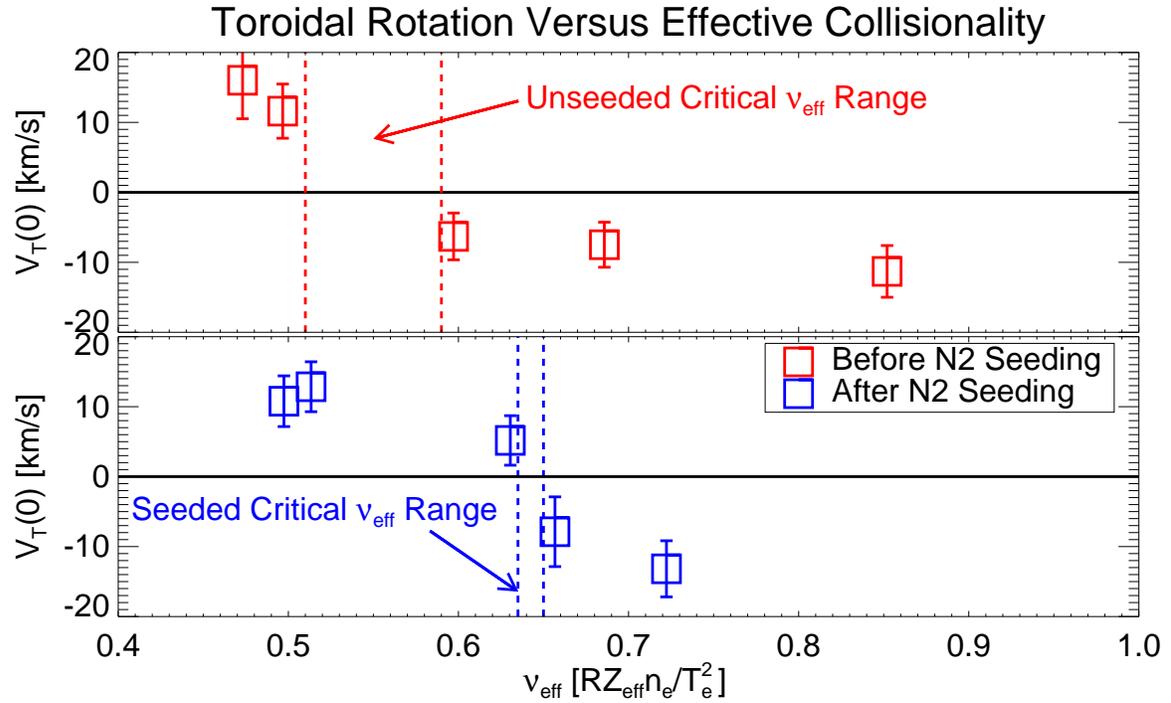
FIG. 11. Plot of the core toroidal rotation velocity versus effective collisionality. Red symbols denote the core toroidal rotation before the nitrogen seeding, while blue symbols denote the core toroidal rotation after the nitrogen seeding. Positive V_{Tor} corresponds to co-current directed rotation and negative V_{Tor} corresponds to counter-current directed rotation.
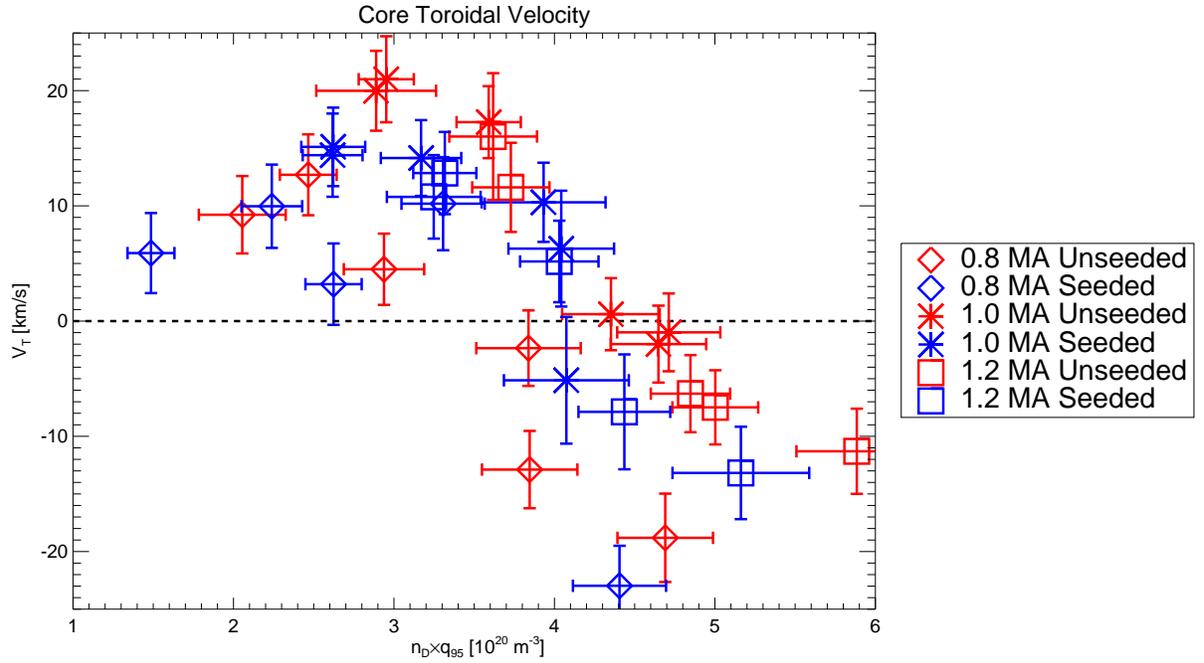
FIG. 12. Plot of the core toroidal rotation velocity versus $n_D q_{95}$ (which is proportional to ν^*) for plasmas before the nitrogen seeding (red) and after nitrogen seeding (blue). Plasmas with $q_{95} = 4.2$ are represented by the diamonds, plasmas with $q_{95} =3.9$ are represented by the stars, and plasmas with $q_{95} =3.4$ are represented by the squares. Positive V_T represents co-current velocities, while negative V_T represents counter-current velocities.